10.1 AN OVERVIEW OF THE 2012 NOAA HAZARDOUS WEATHER TESTBED SPRING FORECASTING EXPERIMENT

John S. Kain, I. L. Jirak,[+] A. J. Clark,[#,*] M. C. Coniglio,* S. J. Weiss,[+] J. Correia Jr.,[#,+] A. R. Dean,[+] P. T. Marsh,[+] C. J. Melick,[#,+] S. D. Miller Jr.,[&,*] R. Sobash,[&,*] M. Xue,[@,&] F. Kong,[@,&] K. W. Thomas,[@,&] V. Lakshmanan,[#,*] D. D. Turner,* D. A. Imy,[$] and S. R. Dembek[#,*]*

**NOAA/OAR/National Severe Storms Laboratory, Norman, OK*
[+]NOAA/NWS/NCEP/Storm Prediction Center, Norman, OK
[#]Cooperative Institute for Mesoscale Meteorological Studies, University of Oklahoma, Norman, OK
[&]University of Oklahoma, School of Meteorology, Norman, OK
[@]Center for Analysis and Prediction of Storms, University of Oklahoma, Norman, Oklahoma
[$]NOAA/NWS/NCEP/Storm Prediction Center, Norman, OK - retired

1. INTRODUCTION

Annual NOAA/Hazardous Weather Testbed (HWT) Spring Forecasting Experiments (SFEs) are organized by the NOAA/OAR/National Severe Storms Laboratory (NSSL) and NOAA/NWS/NCEP/Storm Prediction Center (SPC). These experiments are designed to accelerate the transfer of promising new tools from research to operations and inspire new initiatives for operationally relevant research using a paradigm based on a combination of systematic experimental forecasting activities and evaluation of both raw and post-processed numerical model output. During the 2012 SFE (hereafter SFE12), conducted 7 May through 8 June, several new activities/emphases were introduced, revealing new insights and avenues for innovative research and development.

Experimental forecasting activities were similar to those of recent years but with a new emphasis on temporal trends and variability – and separate, but overlapping "operational" and "development" initiatives for forecast improvement that have near-term and longer-range prospects for operational implementation, respectively. The operational component focused on new forecasting strategies for severe convective weather, including an innovative automated technique that used numerical guidance from a high resolution ensemble to add enhanced temporal resolution to longer-period probabilistic SPC Convective Outlooks, creating a series of consecutive 4-h outlooks. The development component explored issues related to convection initiation (CI), including challenges associated with both timing and location of first storms in a limited forecast domain and issues related to timing of potential societal impacts (e.g., severe convection).

Model-based evaluation activities that were new for 2012 included 1) a more detailed and thorough comparison of sensitivities to microphysical parameterizations in the WRF model (Skamarock et al. 2008), including evaluation of differences in both simulated reflectivity and simulated satellite imagery fields, 2) evaluation of diagnostic algorithms for convection initiation, 3) subjective assessments of forecast guidance for severe-weather parameters from three different high-resolution ensembles, and comparison of calibrated severe-weather guidance products from NCEP's convection-parameterizing Short-Range Ensemble Forecast system (SREF - Du et al. 2009), and the SPC's convection-allowing Storm-Scale Ensemble of Opportunity (SSEO – Jirak et al 2012a).

For the first time in a SFE, a significant comparison of observational systems was included in subjective evaluations during SFE12. This comparison involved observing platforms for severe-weather forecasting applications, including a microwave radiometer (MWR) developed by Radiometrics Corporation and a radiosonde system developed by InterMet Systems. The goals were to 1) compare lower-tropospheric temperature and humidity profiles retrieved by the MWR to in-situ radiosonde measurements and 2) compare full-tropospheric thermodynamic and wind measurements from the InterMet system to the Vaisala RS-92 radiosonde system that is widely used for research, and (when available) to the Sippecan radiosonde system that is used operationally by the National Weather Service (NWS). In addition, the radiosonde profiles were used to evaluate five planetary boundary layer (PBL) parameterizations available in the WRF model, focusing on the ability of the observing systems and the WRF PBL schemes to depict the growth of the convective PBL within regimes of moisture return and moist-convective PBLs prior to convective development.

The purpose of this paper is to provide a high-level overview of SFE12 and document the datasets and collaborators that were important components of the experiment. Further details about individual elements and preliminary results from the experiment will be provided in other presentations and papers from the 2012 AMS Severe Local Storms Conference.

Corresponding author address: John S. Kain, NOAA/OAR/National Severe Storms Laboratory, 120 David L. Boren Blvd., Norman, OK 73072; e-mail: Jack.Kain@noaa.gov

2. PARTICIPANTS AND DAILY ACTIVITIES

A group of approximately 10 NSSL scientists and SPC forecasters/scientists was responsible for conducting daily operations during the 5-week period of SFE12. Groups of 8-10 visitors participated in daily activities (Table 1) for one week (M-F) at a time. These groups were designed to have diverse representation from the scientific and operational-forecasting communities (Table 2). All activities were conducted with full-group participation except for experimental forecasting, for which visitors were randomly assigned to CI or Severe forecasting teams each day. Our goal was to have no more than 3-4 external visitors on any forecast team as a way of ensuring that each visitor was actively engaged in all activities. Both the CI and Severe forecast teams were led by experienced SPC forecasters every day.

Time	Activity
0800-0915	Review of previous day/overnight convective activity, Evaluation of previous day experimental forecast products
0915-1000	Manual analysis of Day 1 large-scale conditions, concluding with group discussion
1000-1200	Break up into "CI" and "Severe" Forecast Teams, with external visitors randomly assigned to different teams
1200-1300	Lunch/preparation for public briefing
1300-1330	Public briefing
1330-1600	Consolidate teams, begin afternoon evaluation activities

Table 1: Summary of daily activities for SFE12

Category	Number of Participants on a given day
Operational SPC Forecasters	1-2
Operational WFO Forecasters	1-2
NSSL Scientists	1-2
Other NOAA/NASA Scientists	1-2
International Scientists/Forecasters And Private Industry	1-2
Academia	1-2

Table 2: Guidelines for participant representation during SFE12

3. DATA

3.1. Experimental Numerical Forecast Systems

3.1.1 CAPS Storm Scale Ensemble Forecast (SSEF) System

As in recent years, the cornerstone of the experimental model guidance for SFE12 was a CONUS-scale high-resolution ensemble forecast system with 4-km grid spacing, 51 vertical levels, and no parameterized convection. The configuration of this system, locally known as the Storm Scale Ensemble Forecast (SSEF) system, was designed in a collaborative effort by scientists and forecasters at the University of Oklahoma (OU) Center for Analysis and Prediction of Storms (CAPS), the SPC, and NSSL. Most of the SSEF members used the WRF-ARW dynamic core (Skamarock et al. 2008. Additional members used the WRF-NMM dynamic core (Janjic 2003), the ARPS model (Xue et al. 2001), and the COAMPS model (Chen et al. 2003).

All members used the 0000 UTC analysis

from the North American Mesoscale (NAM) model (Rogers et al. 2009) as a first-guess field in the initialization process. In some of the WRF-ARW members initial and lateral-boundary conditions (IC/LBCs) were varied by introducing perturbations derived from the operational SREF modeling system. In this subset of perturbed members, model physical parameterizations also varied from member to member. In another subset of WRF-ARW members, IC/LBCs were not perturbed, but model physical parameterizations were systematically varied from member to member so that sensitivities to physical parameterization could be evaluated over the course of the experiment. The members of this subset were collectively referred to as the "physics members", comprised of one group with varying microphysical parameterizations ("the MP members") and another group in which the parameterization of turbulent mixing varied according to member ("the PBL members"). In a third subset mesoscale perturbations were introduced using stochastic kinetic energy backscatter perturbations (i.e., the SKEB members – see Shutts 2005). Finally, storm-scale perturbations were introduced into the initial conditions of all but one member using the CAPS 3DVAR/ARPS Cloud analysis scheme (Xue et al. 2003, 2008; Gao et al. 2004; Kong et al. 2008), which utilized WSR-88D radar reflectivity and radial velocity, along with available surface and upper air observations. Details of the SSEF configuration are summarized in Table 3.

Execution of the SSEF was controlled by CAPS, using computer resources at the University of Tennessee National Institute for Computational Sciences (NICS) and at the University of Oklahoma. Real-time, 36-h forecast output was available at hourly intervals (with higher time frequency output for a limited selection of 2D fields) before 1200 UTC each day. A detailed description of the SSEF modeling system and logistics for real-time integrations and dissemination are available at here.

3.1.2 SPC Storm Scale Ensemble of Opportunity (SSEO)

The SSEO is a 7-member, convection-allowing ensemble consisting of deterministic models available operationally to SPC (Table 4). This "poor man's ensemble" provides a practical alternative to a formal/operational storm-scale ensemble which will not be available in the near-term because of computational/budget limitations. As with the SSEF system, hourly maximum storm-attribute fields, such as simulated reflectivity, updraft helicity, and 10-m wind speed (Kain et al. 2010) are produced from the SSEO, and these fields are used to produce probabilistic guidance for severe weather. Member specifications are provided in Table 4. Members marked with "-12h" in the Model column are 12h time-lagged members, initialized 12h earlier than the other members. All members are initialized with a "cold-start" from the operational NAM – i.e., no radar data assimilation or cloud model is used to produce ICs.

3.1.3 Air Force Weather Agency (AFWA) 4-km ensemble

The Air Force Weather Agency (AFWA) provided output from a recently implemented real-time 10-member 4-km WRF-ARW ensemble (McCormick et al. 2012). Forecasts were initialized at 0000 UTC using 6 or 12 hour forecasts from four global models. Diversity in the AFWA ensemble was achieved through IC/LBCs from the different global models and varied microphysics and boundary layer parameterizations. AFWA ensemble member specifications are provided in Table 5.

3.1.4 NSSL-WRF Model

Forecasters from the SPC and throughout the National Weather Service have used output from the experimental 4 km WRF-ARW produced by NSSL since the fall of 2006. This WRF model is run twice daily at 00 and 12 UTC throughout the year over a full CONUS domain with forecasts to 36 hrs (Kain et al 2010). Output is available online here and here.

3.1.5 GSD High Resolution Rapid Refresh (HRRR) Model

The experimental 3-km grid-spacing HRRR model (Alexander et al. 2010) is nested within the hourly development version of the 13 km Rapid Refresh (RAP model), which provides IC/LBCs for the HRRR. The HRRR uses a version of the WRF-ARW with a physics package very similar to the RUC model (Benjamin et al. 2004). A unique aspect of the RAP is the hourly GSI data assimilation system that incorporates a wide array of observational datasets including radar reflectivity via the radar-Diabatic Digital Filter Initialization. The HRRR integration is run hourly over a full CONUS domain with forecasts to 15 hrs. In 2012, at the initial time the simulated HRRR reflectivity came from a 1-hr RAP forecast; downscaling from the RAP 13 km grid to the HRRR 3 km grid occurred very quickly during the first hour.

Member	IC	BC	Microphy	LSM	PBL
arw_cn	00Z ARPSa	00Z NAMf	Thompson	Noah	MYJ
arw_c0 (18h)	00Z ARPSa	00Z NAMf	Thompson	Noah	MYJ
arw_m3	+ em-p1_pert	em-p1	Morrison	RUC	YSU
arw_m4	+ nmm-n2_pert	nmm-n2	Morrison	Noah	MYJ
arw_m5	+ em-n2_pert	em-n2	Thompson	Noah	ACM2
arw_m6	+ rsm-n2_pert	rsm-n2	M-Y	RUC	ACM2
arw_m7	+ nmm-p1_pert	nmm-p1	WDM6	Noah	MYNN
arw_m8	+ rsm-p1_pert	rsm-p1	WDM6	RUC	MYJ
arw_m9	– etaKF-n1_pert	etaKF-n1	M-Y	RUC	YSU
arw_m10	+ etaKF-p1_pert	etaKF-p1	WDM6	Noah	QNSE
arw_m11	– etaBMJ-n1_pert	etaBMJ-n1	M-Y	Noah	MYNN
arw_m12	00Z ARPSa	00Z NAMf	Thompson	Noah	MYNN
arw_m13	00Z ARPSa	00Z NAMf	Thompson	Noah	ACM2
arw_m14	00Z ARPSa	00Z NAMf	M-Y	Noah	MYJ
arw_m15	00Z ARPSa	00Z NAMf	Morrison	Noah	MYJ
arw_m16	00Z ARPSa	00Z NAMf	WDM6	Noah	MYJ
arw_m17	00Z ARPSa	00Z NAMf	Thompson	Noah	QNSE
arw_m18	00Z ARPSa	00Z NAMf	Thompson	Noah	YSU
arw_m19*	00Z ARPSa	00Z NAMf	Thompson	Noah	MYJ
arw_m20*	+ em-p1_pert	em-p1	Morrison	RUC	YSU
arw_m21*	– rsm-n2_pert	rsm-n2	M-Y	RUC	ACM2
arw_m22*	+ rsm-p1_pert	rsm-p1	WDM6	RUC	MYJ
arw_m23*	+ etaKF-p1_pert	etaKF-p1	WDM6	Noah	QNSE
nmm_cn	00Z ARPSa	00Z NAMf	Ferrier+	Noah	MYJ
arps_cn	00Z ARPSa	00Z NAMf	Lin	force-restore	force-restore
cmps_cn	00Z ARPSa	00Z NAMf	Hobbs-Rutledge	?	?
cmps_c1	00Z ARPSa	00Z NAMf	M-Y	?	?
cmps_c0	00Z ARPSa	00Z NAMf	Hobbs-Rutledge	?	?

Table 3 CAPS SSEF system configuration. For the WRF members, version 3.3.1 is used. NAMa and NAMf refer to the NAM analysis and forecast, respectively (12-km grid-spacing). ARPSa refers to ARPS 3DVAR and cloud analysis. Elements in the IC column followed by a + or – indicate SREF member perturbations added to the control member ICs. All WRF members use RRTM (Mlawer et al. 1997) short-wave radiation and Goddard (Chou and Suarez 1994) long-wave radiation parameterizations. Boundary layer schemes include Mellor-Yamada-Janjic (MYJ; Janjic 1994), YonSei University (YSU; Noh et al. 2003), Mellor-Yamada Nakanishi and Niino (MYNN; Nakanishi and Niino 2009), Quasi-Normal Scale Elimination (QNSE; Sukoriansky et al. 2006), and the Asymmetrical Convective Model version 2 (ACM2; Pleim 2007). Microphysics schemes include Thompson et al. (2008), WRF single-moment 6-class (WSM-6; Hong and Lim 2006), WRF double-moment 6-class (WDM-6; Lim and Hong 2010), Ferrier et al. (2002), Milbrandt and Yau (2005), and Morrison et al. (2005). Ferrier+ refers to an updated version of Ferrier et al. (2002). Land-surface models include the NOAH (Chen and Dudhia 2001), and RUC (Smirnova et al. 1997, 2000). Member names beginning with "cmp" use the Navy COAMPS modeling system. Red-shaded members names denote "core" members. Grey shaded table cells denote "physics members". Pink shaded cells denote SKEB perturbation members.

Member #	Model	Grid-spacing	Agency	PBL	Microphysics	LSM
sseo01	WRF-ARW	4-km	NSSL	MYJ	WSM6	Noah
sseo02	Hi-Res Window WRF-ARW	5.15-km	NCEP/EMC	YSU	WSM3	Noah
sseo03	Hi-Res Window WRF-ARW -12h	5.15-km	NCEP/EMC	YSU	WSM3	Noah
sseo04	CONUS WRF-NMM	4-km	NCEP/EMC	MYJ	Ferrier	Noah
sseo05	Hi-Res Window WRF-NMM	4-km	NCEP/EMC	MYJ	Ferrier	Noah
sseo06	Hi-Res Window WRF-NMM -12h	4-km	NCEP/EMC	MYJ	Ferrier	Noah
sseo07	NMMB Nest	4-km	NCEP/EMC	MYJ	Ferrier+	Noah

Table 4. SSEO member specifications.

Member #	ICs/LBCs	LSM	Micro-physics	PBL
afwa01	18Z UKMET	Noah	WSM5	YSU
afwa02	18Z GFS	RUC	Goddard	MYJ
afwa03	12Z GEM	Noah	Ferrier	QNSE
afwa04	12Z NOGAPS	Noah	Thompson	MYJ
afwa05	18Z UKMET	RUC	Thompson	MYJ
afwa06	18Z GFS	Noah	Thompson	QNSE
afwa07	12Z GEM	Noah	Goddard	YSU
afwa08	12Z NOGAPS	Noah	WSM5	QNSE
afwa09	18Z UKMET	RUC	Ferrier	QNSE
afwa10	18Z GFS	Noah	WSM5	YSU

Table 5. AFWA ensemble member specifications.

3.2 Experimental Observing Systems

Experimental observing systems included a passive microwave radiometer and a GPS-based radiosonde system. Along with an evaluation of the observing systems, datasets from these systems provided observations for the continuing evaluation of five turbulent mixing parameterization options in the SSEF physics members (MYJ, YSU, MYNN, ACM2, and QNSE) that began in SFE11.

3.2.1 Passive Microwave Radiometer

Radiometrics, Inc.. loaned a passive microwave radiometer (MWR, model MP-3000) to researchers at NSSL and OU for evaluation through September 2012. The MWR operates from the roof of the National Weather Center, in which the HWT is located. The HWT/SFE is interested in the capability of the MWR to retrieve vertical profiles of temperature and water vapor for severe weather forecasting applications. A MWR measures the radiation emitted/transmitted by the atmosphere near frequencies sensitive to water vapor and oxygen (Fig. 1). The more opaque channels (i.e., where the atmosphere has a larger optical depth) measure near-surface conditions while the more transparent channels measure conditions higher in the troposphere (Otkin et al. 2011).

A MWR is able to obtain radiance observations in most atmospheric conditions, except in precipitation, as the measurements are essentially insensitive to clouds. The radiance measurements are then "inverted" using statistical or physical retrieval algorithms to obtain temperature and water vapor profiles. The retrievals can be obtained at relatively high temporal resolution, with the MP-3000 providing profiles approximately every 5 minutes (Fig. 2). Accurate, high temporal measurements of the temperature and humidity profiles could be beneficial for severe weather forecasting. However, the spatial (vertical) resolution is limited. Specifically, depending on

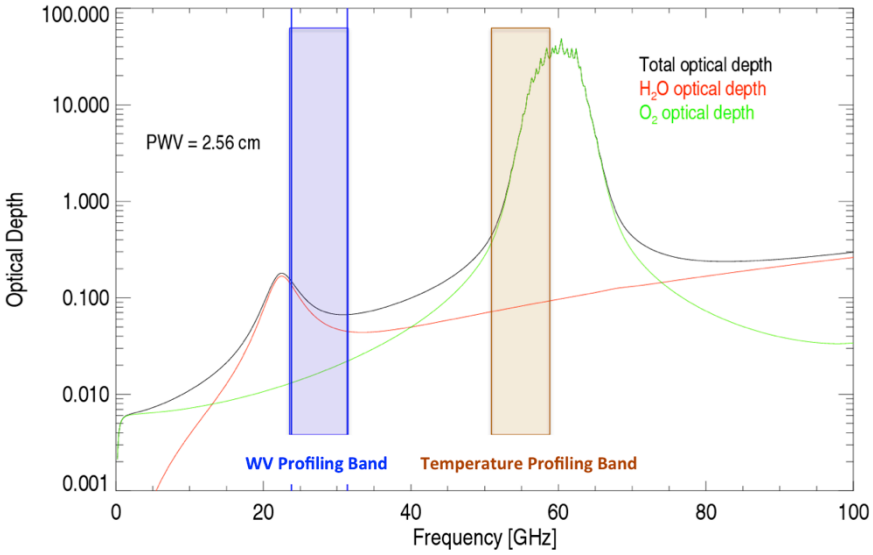

Fig. 1. *Water vapor and oxygen absorption lines and their summed optical depth, along with the bands used by the Radiometrics MWR to measure water vapor and temperature in the atmosphere.*

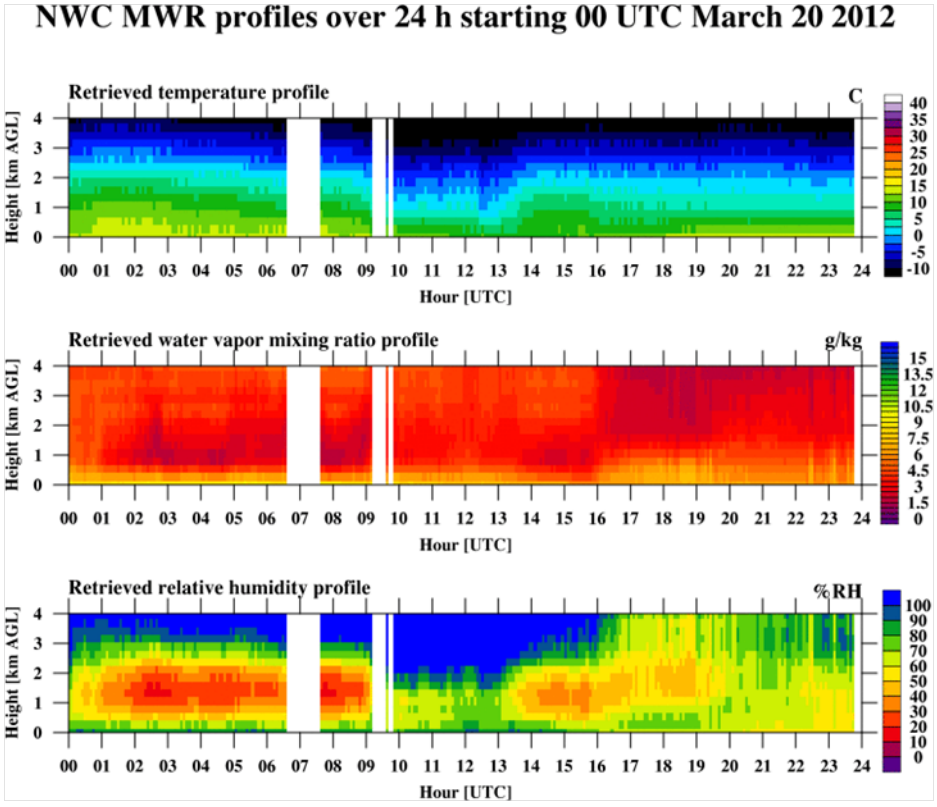

Fig. 2. *An example of 5-minute thermodynamic data from the MP-3000 microwave radiometer, plotted in time-series format.*

.

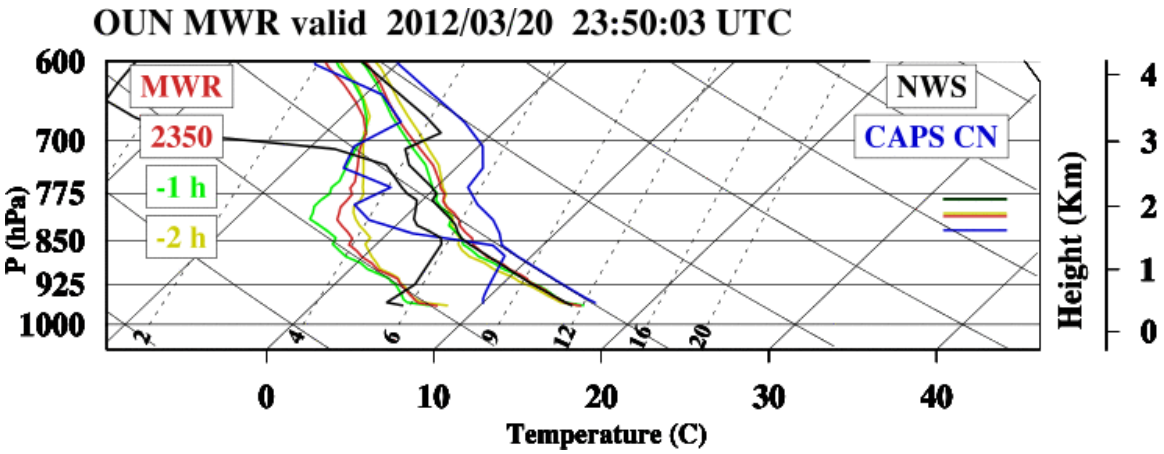

Fig. 3. *SkewT diagram of the NWC MWR profile valid 2350 UTC 20 March 2012 (red lines) and the profiles valid one and two-hours previous (green and yellow lines, respectively), the 24 h forecast for Norman from the control member of the SSEF (blue lines), and the NWS radiosonde observation valid at 0000 UTC 21 March 2012 (black lines). The horizontal lines to the right of the temperature traces show the diagnosed height of the PBL using a version of the RUC algorithm.*

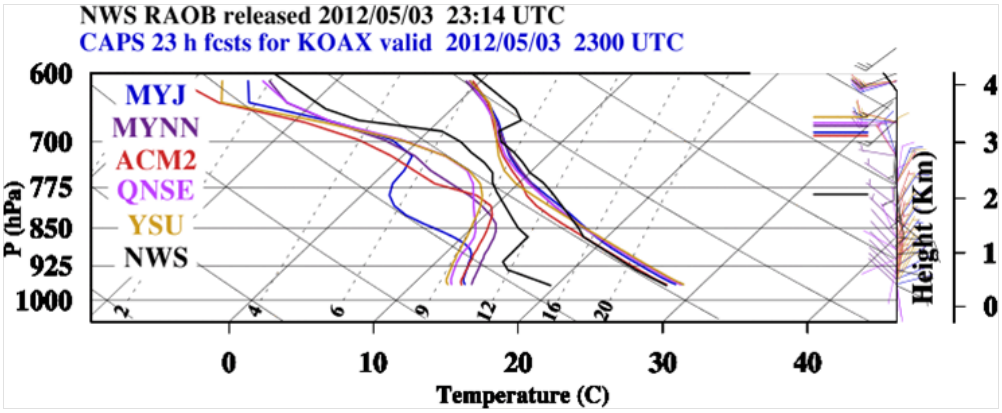

Fig. 4. *23 h forecasts from the five SSEF members that vary only by PBL scheme compared against the NWS radiosonde observation released at ~2300 UTC 3 May 2012 (black line). Horizontal lines on the right of the diagram are as in Fig. 3..*

the scanning strategy and the retrieval algorithm, a MWR can only attain 2 or 3 independent pieces of information in the water vapor profile and only 2 – 4 pieces in the temperature profile in the lower troposphere (Löhnert et al. 2009). Of course, the detailed vertical structure of the temperature and humidity profiles is also important to know, but given the limitations in retrieving the vertical structure of the profiles, it remains to be seen how useful the MWR-derived profiles can be for severe weather forecasting. Instantaneous MWR-derived profiles were compared to radiosonde data on a daily basis during SFE12, focusing on the lower troposphere as shown in Fig. 3.

3.2.2 GPS radiosonde system

Recent technology advances have allowed alternative radiosondes and lower-cost radiosonde ground stations to be competitively marketed compared to the Vaisala RS-92 system, the gold standard for research applications (Nash et al. 2005). One such system (sonde and ground station) by InterMet Systems was purchased by NSSL two years ago for evaluation. InterMet uses a proprietary sonde costing about the same as Vaisala's RS92, but the ground station system can be considerably less expensive. Two different options for the InterMet ground system were used in comparisons with the complete Vaisala RS92 sonde system during SFE12. NSSL is interested in the potential cost savings offered by the InterMet systems, provided that the observations are comparable to the Vaisala measurements.

On selected days during SFE12, i.e., days when a convective boundary layer was expected to develop and especially when deep convection was expected in Oklahoma later in the afternoon,

teams of volunteers launched both the InterMet and Vaisala sondes attached to the same balloon from outside the National Weather Center. The sondes were launched approximately every three hours (1400, 1700, and 2000 UTC nominally) and served three purposes, to 1) evaluate the performance of the InterMet sondes and the two different ground receiver options, 2) provide in situ observations of temperature and water vapor mixing ratio to compare to the MWR profiles, and 3) provide verifying observations for WRF-ARW forecasts of the temperature and moisture profile from the five PBL members of the SSEF at the grid point closest to Norman (e.g., Fig. 4).

4. EXPERIMENTAL FORECASTS

Each morning during SFE12 forecast teams utilized the full range of experimental and operational datasets to manually prepare experimental forecast products.

4.1 Severe Convection

The first task of the Severe forecast team was to prepare a product similar to the 1630 UTC SPC Day-1 Convective Outlook. Specifically, this product contained a prediction for the probability of severe convective weather (i.e., hail, wind, and tornado) within 25 miles of a point and it was issued by 1600 UTC and was valid between 1600 and 1200 UTC the following day. Unlike the CONUS-scale operational SPC Outlooks, this experimental product focused on a regional domain, centered on the mesoscale area of greatest threat for severe convection on a given day, and it did not discriminate between the hail, wind, and tornado threats. Additional probabilistic forecasts were prepared for shorter time windows within this period. In particular, identically formatted outlooks for 20-00, 00-04, and 04-12 UTC were also generated by 1700 UTC.

The full period (16-12 UTC) experimental probabilistic outlook was also used to test the utility of an experimental calibrated temporal disaggregation procedure that automatically breaks down longer-period spatial probabilities into subset-time-period components (Fig. 5) based on calibrated numerical guidance from the SPC's SSEO (Jirak et al. 2012a). This automated procedure was used to generate a second set of 20-00, 00-04, and 04-12 UTC outlooks, which were compared directly to the manual forecasts and observations of severe weather the following morning.

The purpose of this exercise was to determine whether the automated, shorter-time-period forecasts were comparable in skill to the corresponding manual forecasts. If so, this process might have utility in operations, allowing some level of automation to be introduced to produce multiple forecast graphics and enhanced temporal resolution from a single well established, widely used, skillful, manually-generated SPC Outlook product. These automated, temporally focused graphics could be modified manually, providing a useful first draft of a final product and helping to satisfy anticipated needs for increased temporal specificity while minimizing additional workload.

4.2 Convection initiation

Similar to the severe-convection counterpart, the CI forecasting process began with identification of a regional domain within which deep convection was anticipated later in the day (e.g., the area outlined by the brown rectangle in

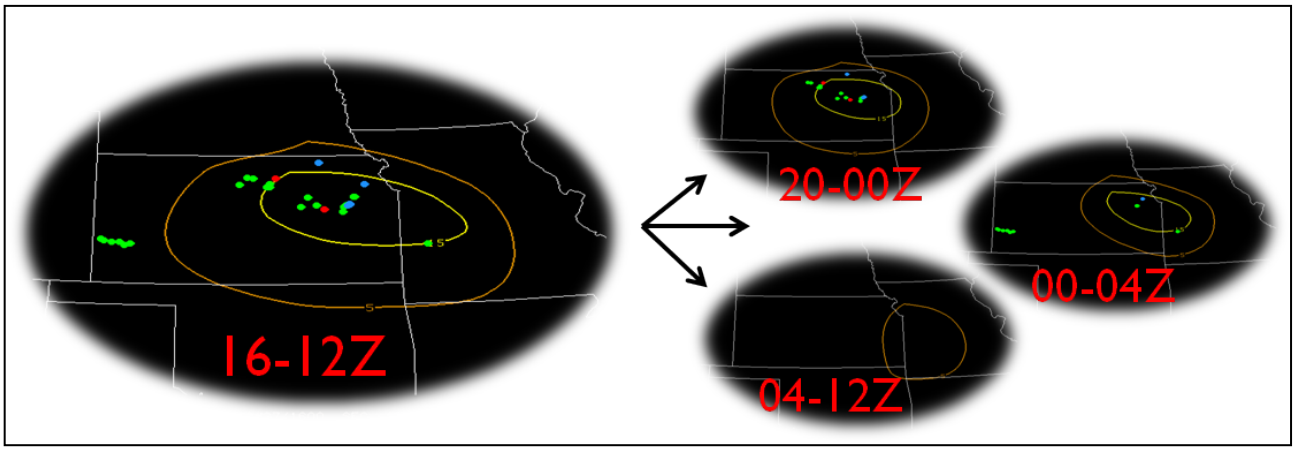

Fig. 5. *A conceptual representation of the automated temporal disaggregation of probabilistic convective outlooks. Dots indicate locations of severe hail (green), wind (blue), and tornado reports during the valid time periods.*

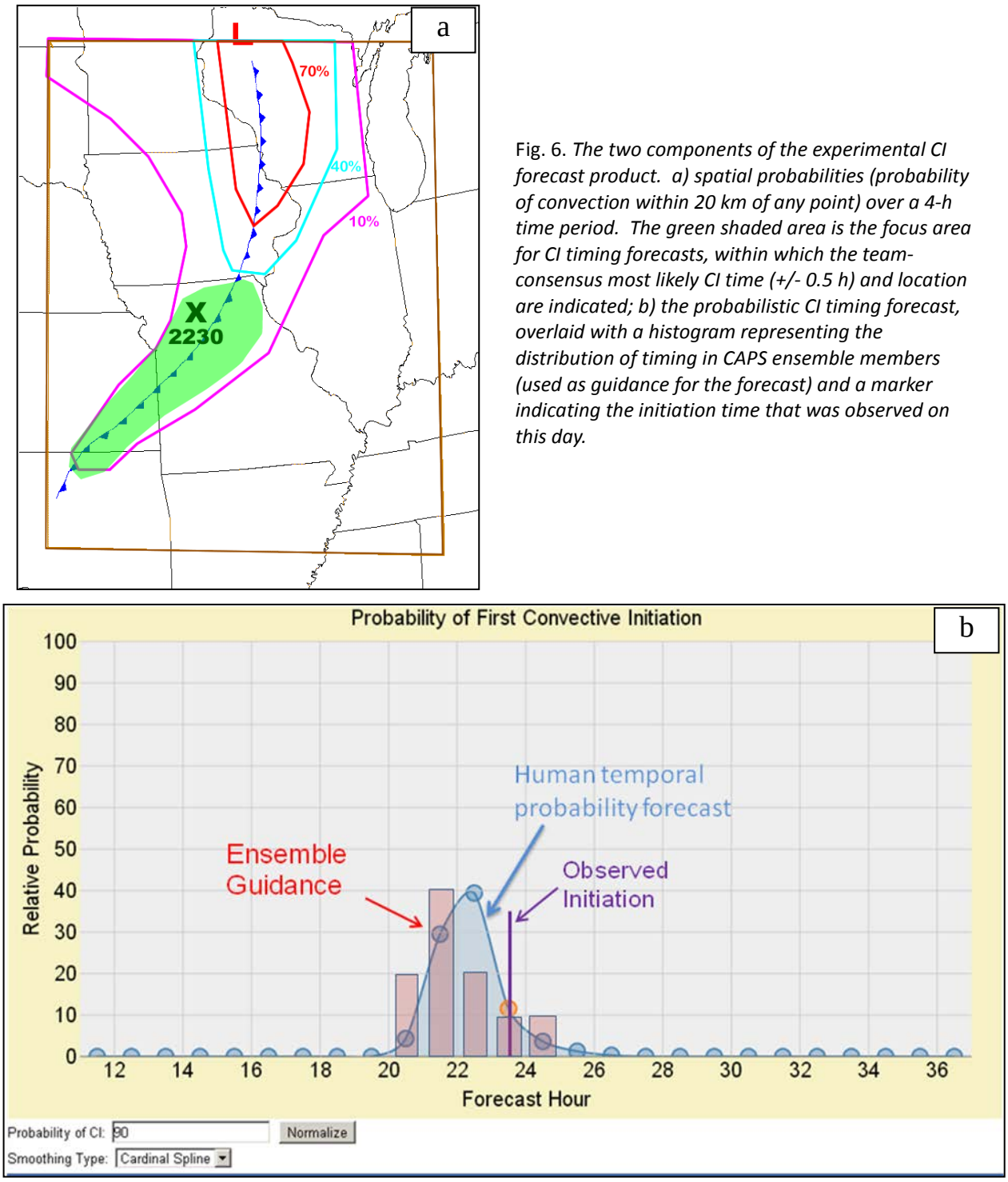

Fig. 6. *The two components of the experimental CI forecast product. a) spatial probabilities (probability of convection within 20 km of any point) over a 4-h time period. The green shaded area is the focus area for CI timing forecasts, within which the team-consensus most likely CI time (+/- 0.5 h) and location are indicated; b) the probabilistic CI timing forecast, overlaid with a histogram representing the distribution of timing in CAPS ensemble members (used as guidance for the forecast) and a marker indicating the initiation time that was observed on this day.*

Fig. 6a). This process also included an element that was directly analogous to an operational SPC product, in this case the SPC Thunderstorm Outlook. Specifically, like the Thunderstorm Outlook, the experimental forecasts contained probability contours indicating the likelihood of a thunderstorm(s) within 20 km of a point during a specified time period. The contour levels were 10%, 40%, and 70% (e.g., Fig. 6) and the time periods were 16-20, 20-00, and 00-04 UTC.

In addition, there was a more refined emphasis on the timing of CI, designed to target initiation associated with a specific forcing mechanism. For this component, a limited sub-domain was selected within the larger regional domain, with the goal of isolating an anticipated specific CI episode from any nearby convection that was pre-existing and/or associated with a different forcing mechanism. The sub-domain was clearly identified on the experimental forecast graphic that was valid during the time period within which the targeted CI episode was

expected to occur. The CI forecast team came to consensus on 1) the most likely time (hourly interval) and location of CI, 2) the overall probability that the targeted CI episode would occur, and 3) an estimate of uncertainty in the timing, given the occurrence of the episode. The consensus location and hour were indicated on the forecast graphic with an "X" and time (labeled as the midpoint of the hour), respectively (Fig. 6a). Uncertainty information was indicated on a separate graphic, using a web-based interactive display (Fig. 6b). This display allowed the CI forecast team to create a temporal probability distribution by simply dragging markers associated with each forecast hour to graphical positions representing the relative likelihood of CI at individual hours. It included a normalization function that adjusted the total area represented by the hourly probabilities based on the overall likelihood of the CI episode, while maintaining relative hourly amplitudes.

The ten core members of the CAPS ensemble were used to provide specific numerical guidance for the temporal probability forecasts. Specifically, using the automated CI-detection algorithm described in Kain et al. (2013) and Clark et al. (2012a), a histogram of predicted CI timing was generated by searching for the first-CI event in each member within the forecast sub-domain and within +/- 5 h of the preliminarily forecasted CI time (e.g., Fig. 6b)

5. RESULTS

5.1 Overview

Many results from SFE12 are reported elsewhere and will not be reproduced here. For example, Jirak et al. (2012b) discuss the experimental severe-convection forecasts and evaluate the utility of the temporal disaggregation approach; Miller et al. (2012) and Marsh et al. (2012) discuss the CI forecasts and a preliminary assessment of the skill of these forecasts; Coniglio et al. (2012) report preliminary results from comparisons of different sonde systems and vertical profiles derived from microwave radiometers while Coniglio et al. (2013) demonstrate PBL-scheme sensitivities in forecast-sounding profiles; Jirak et al. (2012a) suggest that the SSEO was at least as skillful as the more formally constructed SSEF and AFWA ensemble systems during SFE12; Melick et al. (2012) discuss objective verification strategies and results.

5.1.1 Sensitivities related to Microphysical Parameterization.

There has been comparatively little formal analysis of sensitivities to microphysical parameterization (MP). Clark et al. (2012b) diagnosed the properties, propagation speeds, etc. of precipitation features predicted during SFE12 as a function of MP, but the sensitivity of output fields such as simulated reflectivity and brightness temperature to MP, which was assessed on a daily basis during SFE12, is not reported elsewhere. This results section highlights some of the sensitivities that were noted during those daily assessments.

5.1.1.1 Simulated Reflectivity Algorithm

Before the start of SFE12, organizers worked with developers of the Thompson (Thompson et al. 2008), Morrison (Morrison et al. 2005), and WDM6 (Lim and Hong 2010) MPs to formulate simulated-reflectivity algorithms that were uniquely designed for these three double-moment MPs. Earlier experiments had used the formulation described in Kain et al. (2008), which is appropriate for the WSM6 MP (Hong et al. 2004) but inadequate in accounting for the unique parameter settings, size distributions, and assumptions that are prescribed in different MPs in the WRF model. Simulated reflectivity fields derived from the "new" and "old" methods were compared to observations on a daily basis and the impact of the change was clearly evident, more so with some MPs than with others. For example, a snapshot of composite reflectivity from 27-h forecasts valid 0300 UTC 31 May suggests that the character of differences between the "new" and "old" output fields varies from one MP to another (Fig. 7). One can compare these output fields for different times and dates by clicking here. During SFE12, the old calculation was used only for quick comparisons like those enabled by Fig. 7. The new MP-specific calculations were used for most purposes and they will be used exclusively from this point forward in this summary.

5.1.1.2 Simulated Composite Reflectivity

The sensitivity of composite reflectivity (CREF) to MP was quite revealing (Fig. 8). For example, the hourly-maximum (maximum value at each grid point during the preceding hour – hereafter HM) CREF field from the M-Y MP tended to produce the highest coverage of very high reflectivity values (> 60 dBZ), the Morrison scheme often produced relatively large areas of moderately high (35-45 dBZ) values and fewer very high values than the others. The HM-CREF fields associated with the Thompson and WDM6 schemes were not so easy to characterize in terms of systematic biases. These fields can be compared for additional dates and times here.

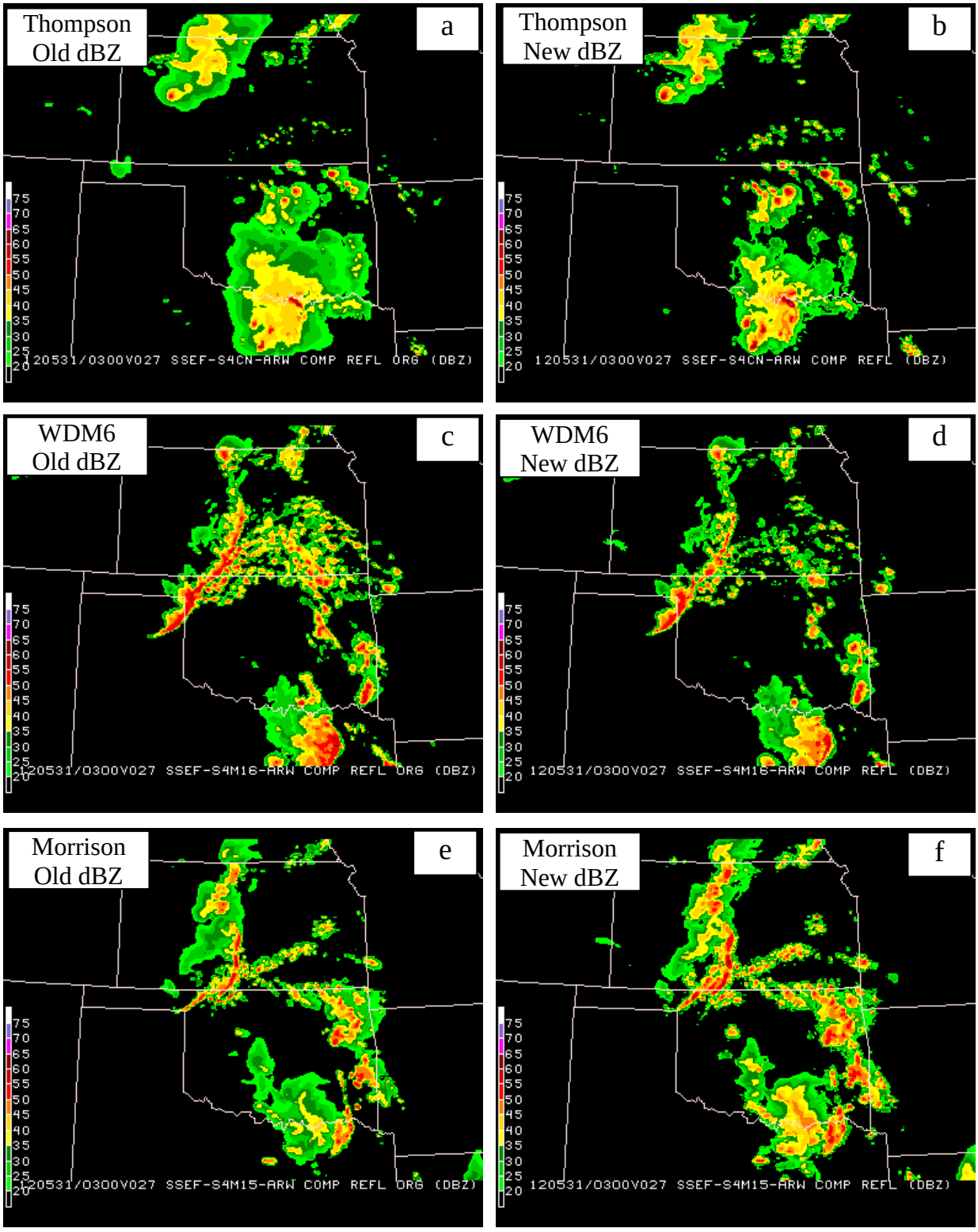

Fig. 7. *Comparative example of simulated reflectivity fields derived from the "old" (Kain et al. 2008) reflectivity calculation (left side) and the new, MP-consistent calculation (right side) for the Thompson (a, b), WDM6 (c, d), and Morrison (e, f) MPs.*

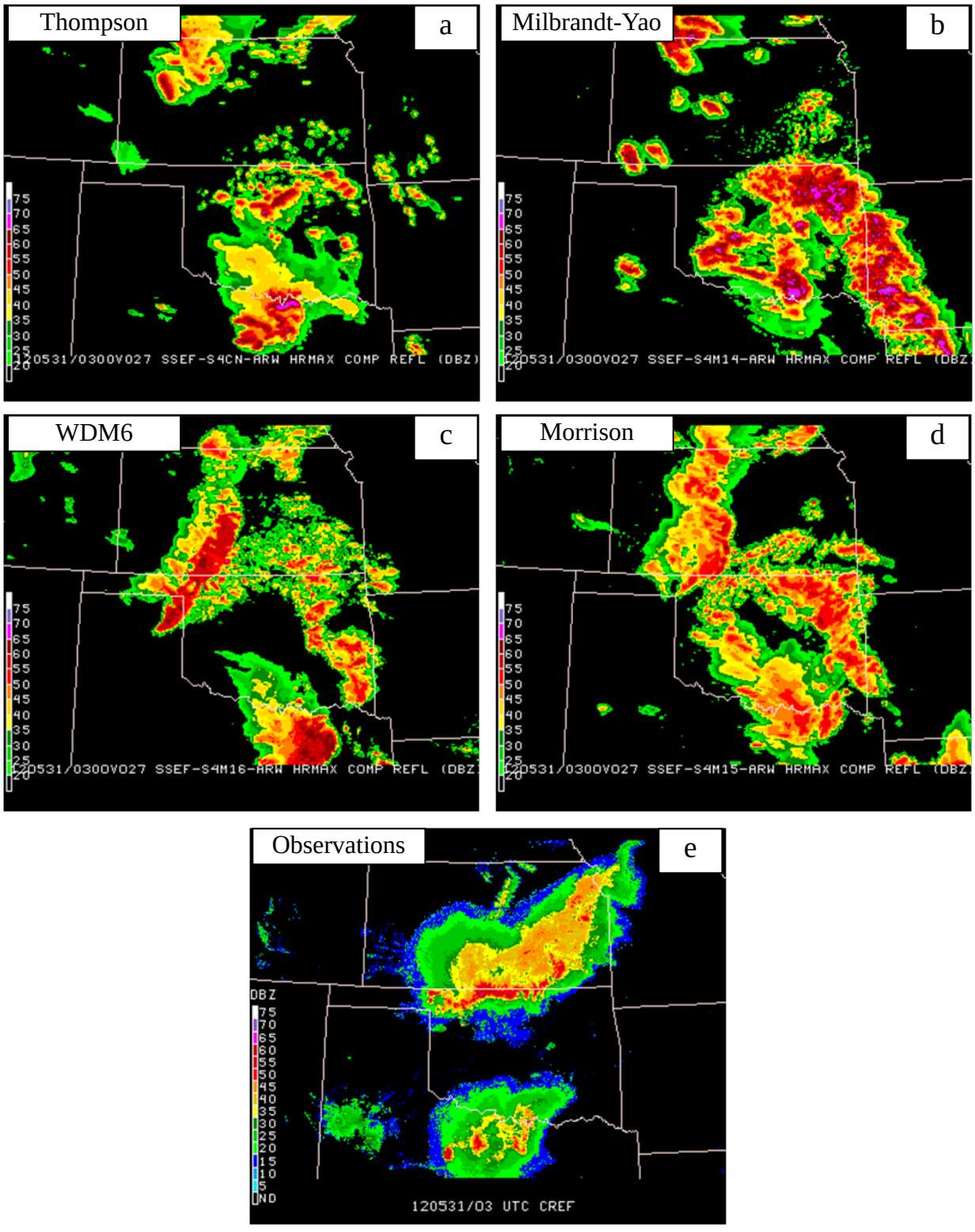

Fig. 8. *Example of differences in simulated HM-CREF (see text) as a function of MP, showing a) Thompson, b) Mibrandt-Yau, c) WDM6, d) Morrison, and e) observed HM-CREF.*

5.1.1.3 Simulated Reflectivity at -10º C

Simulated reflectivity fields at the -10º C temperature level (hereafter MTR) were compared every day as well because grid-point values greater than or equal to 35 dBZ were used as proxies for convectively-active (CA) grid points. The same concept was applied to observed reflectivity fields (see Roberts and Rutledge 2003; Mecikalski and Bedka 2006; Gremillion and Orville 1999). Figure 9 provides an example of HM-MTR fields associated with the MP schemes discussed above. In the context of the CA diagnosis that was a fundamental part of the CI component of SFE12, the HM-MTR field provides a quick visual assessment of points that were CA during the preceding hour (the yellow and "hotter" colors). Although it is not quantitatively evident from figure 9, each of the MPs tended to over-predict the coverage of MTR exceeding 35 dBZ, and thus the coverage of CA. Coverage-bias statistics for diagnosed CA points, computed over "severe" forecast domains and aggregated for the last 20 days of the experiment indicated that bias ranged from 1.8 (Thompson scheme) to 4.1 (Morrison scheme). This high bias had consequences for the CI component of SFE12. Specifically, as discussed in Miller (2013), probabilistic numerical guidance for CA coverage was inflated, and this may have had a detrimental impact on guidance products for CI as well (see Miller et al. 2012). Aside from the coverage of MTR ≥ 35 dBZ, participants in SFE12 noted that the Thompson MP typically produced the highest HM-MTR values for a given event. These sensitivities can be explored for other dates and times here.

5.1.1.4 Simulated Reflectivity Histograms

After examining simulated reflectivity fields from different perspectives during the first couple of weeks during SFE12, it became evident that the various MPs have systematic differences in the way that they distribute reflectivity values across the spectrum of possible values. During the remainder of the experiment this aspect of the MP sensitivity was explored by creating histograms of simulated (and observed) reflectivity values each day. These histograms were populated by counting the occurrence of reflectivity values in each 2-dBZ bin over the range of 0 – 80 dBZ aggregated from grid points over the entire forecast-output domain, the 1200 - 1200 UTC period (12-36 h forecast period for the models), and hourly snapshots. They were created for each of the physics members of the CAPS ensemble, four of which used the Thompson MP with unique PBL schemes (i.e., the PBL members) while the other three used the Morrison, M-Y, and WDM6 MPs but were identically configured otherwise. As expected, the distributions of simulated reflectivity varied significantly as a function of MP. For example, for the 24-h period starting1200 UTC on 25 May 2012, all of the PBL/Thompson members produced a distinctive peak in frequency between about 15-20 dBZ, in rough agreement with a peak in observations. This was true from both a low-level (Fig. 10a) and column-maximum (composite - Fig. 10b) perspective. These members also produced a discernible secondary peak between about 40 and 45 dBZ, but with no obvious observational counterpart in that range. In contrast, none of the other MPs seemed to produce this higher-reflectivity secondary peak. The Morrison scheme produced a broader lower-reflectivity peak than did the PBL/Thompson members and there were hints of this peak in the WDM6 distribution, but the M-Y distribution was closer to one of exponential decay as dBZ increased. In terms of distribution amplitude (a measure of areal coverage) the simulated values were significantly higher than observed in almost all bins. This is consistent with the high coverage bias that was noted above for the 35 dBZ threshold of the HM-MTR. Additional reflectivity histograms can be explored by clicking here

5.1.1.5 Simulated Satellite Imagery

Another aspect of the daily assessment of MP sensitivities involved simulated satellite imagery, specifically infrared brightness temperature (see Bikos et al. 2012). As with reflectivity, this assessment indicated a strong sensitivity to MP. As is the case in the example shown in Figure 11, the M-Y MP typically produced more extensive, colder cloud shields than the other three MPs, while WDM6 was often associated with the smallest areal coverage of brightness-temperature less than 211 K (green color-fill) and more spotty coverage than the other MPs. By comparison the Thompson and Morrison MPs tended to produce brightness-temperature fields with similar coverage and general appearance. During SFE12, it was noted that these implied differences in cloud coverage/opacity were associated with differences in temperature of the land surface and the lower troposphere, apparently due to cloud radiative impacts. Clearly, these differences could have significant impacts on the evolution of convective systems and subsequent convective development at a given location. These fields can be explored for other dates and times here.

,

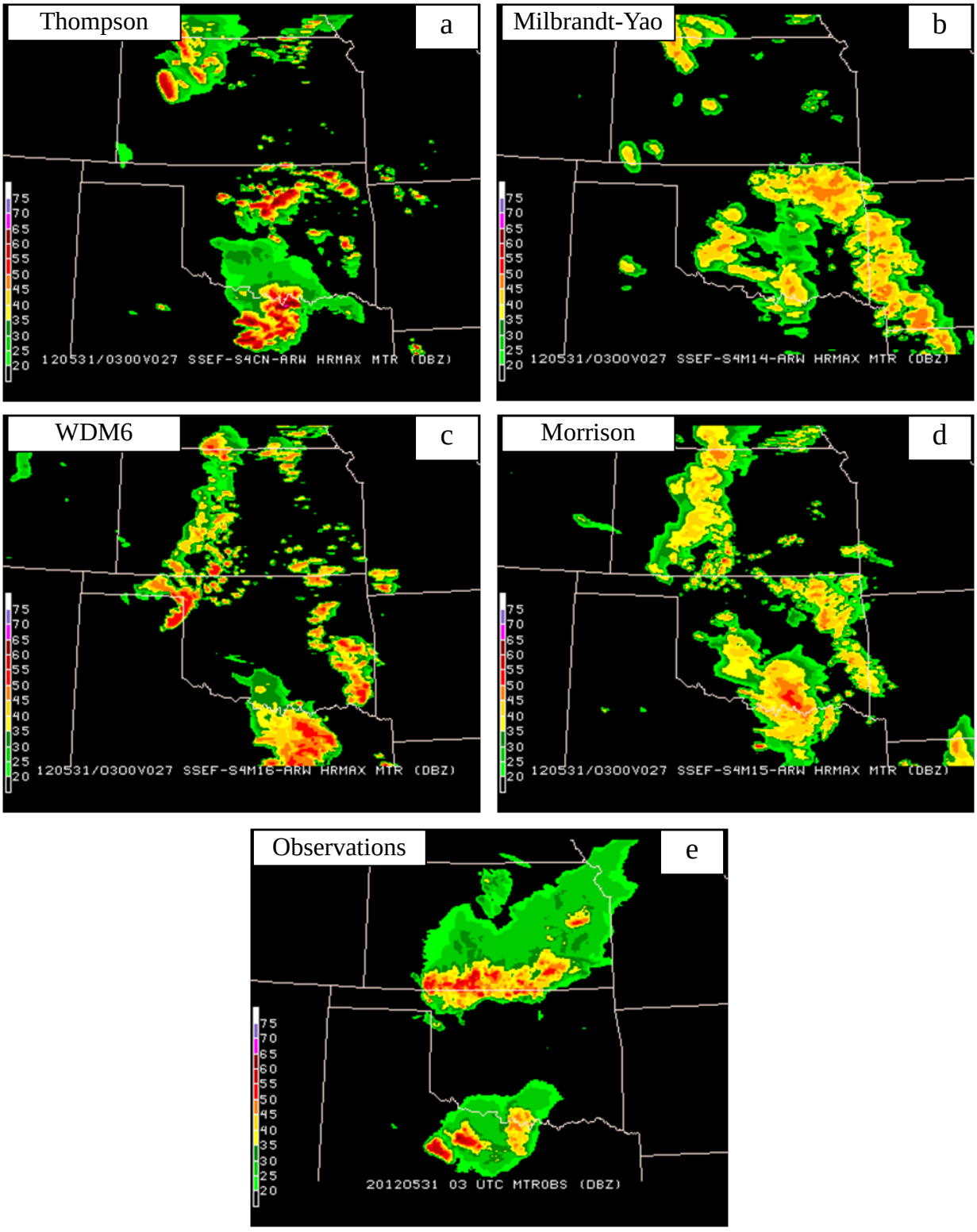

Fig. 9. *As in Fig. 8, but for the simulated and observed HM-MTR fields (see text).*

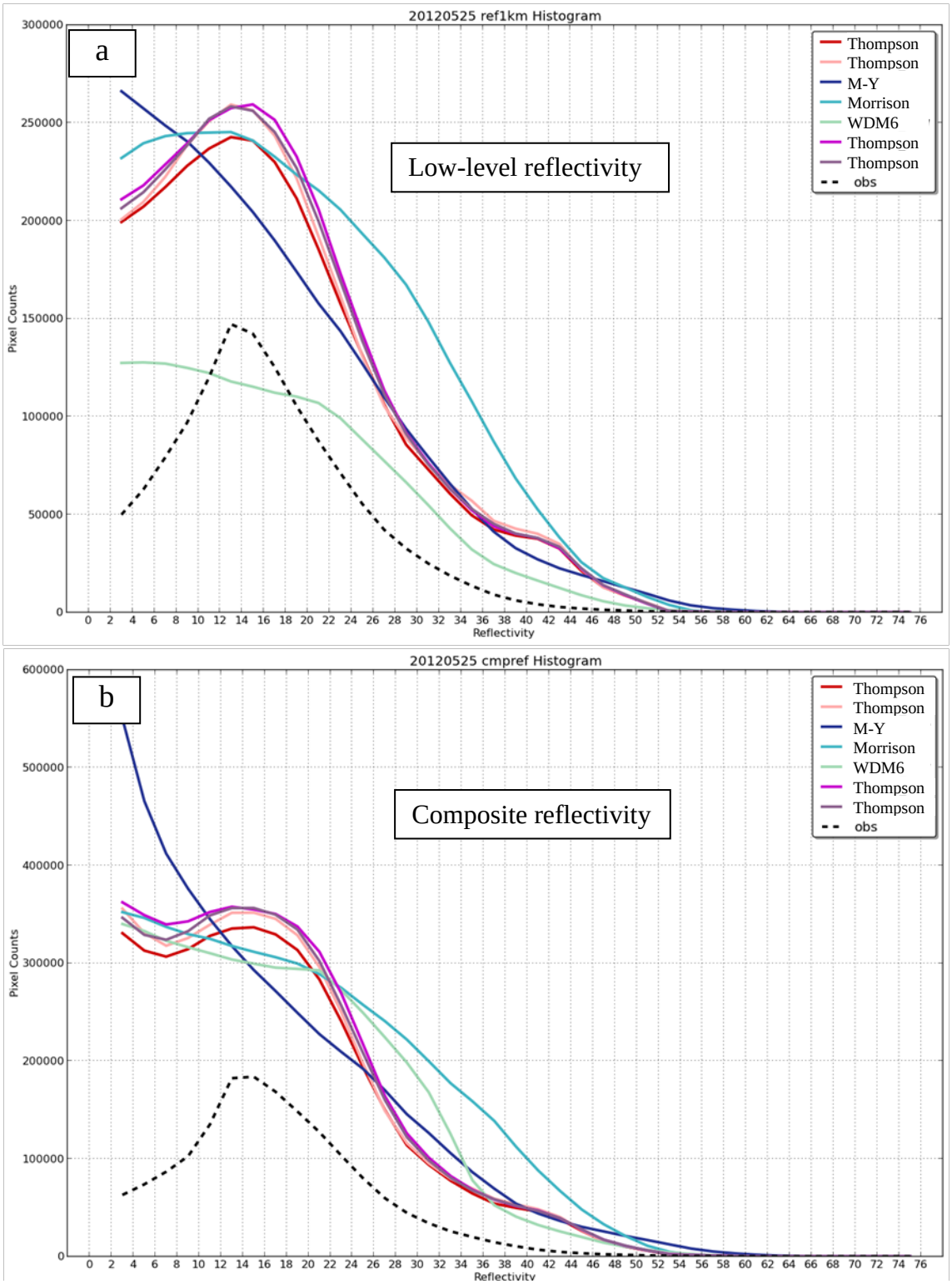

Fig. 10. *Examples of reflectivity histograms as a function of microphysical parameterization for the Physics members of the CAPS ensemble. The curves represent the grid-point count in each 2-dBZ reflectivity bin, derived from the 24-h forecast/observation period starting at 1200 UTC on 25 May 2012, based on hourly snapshots and including all grid points in the full CAPS output domain.*

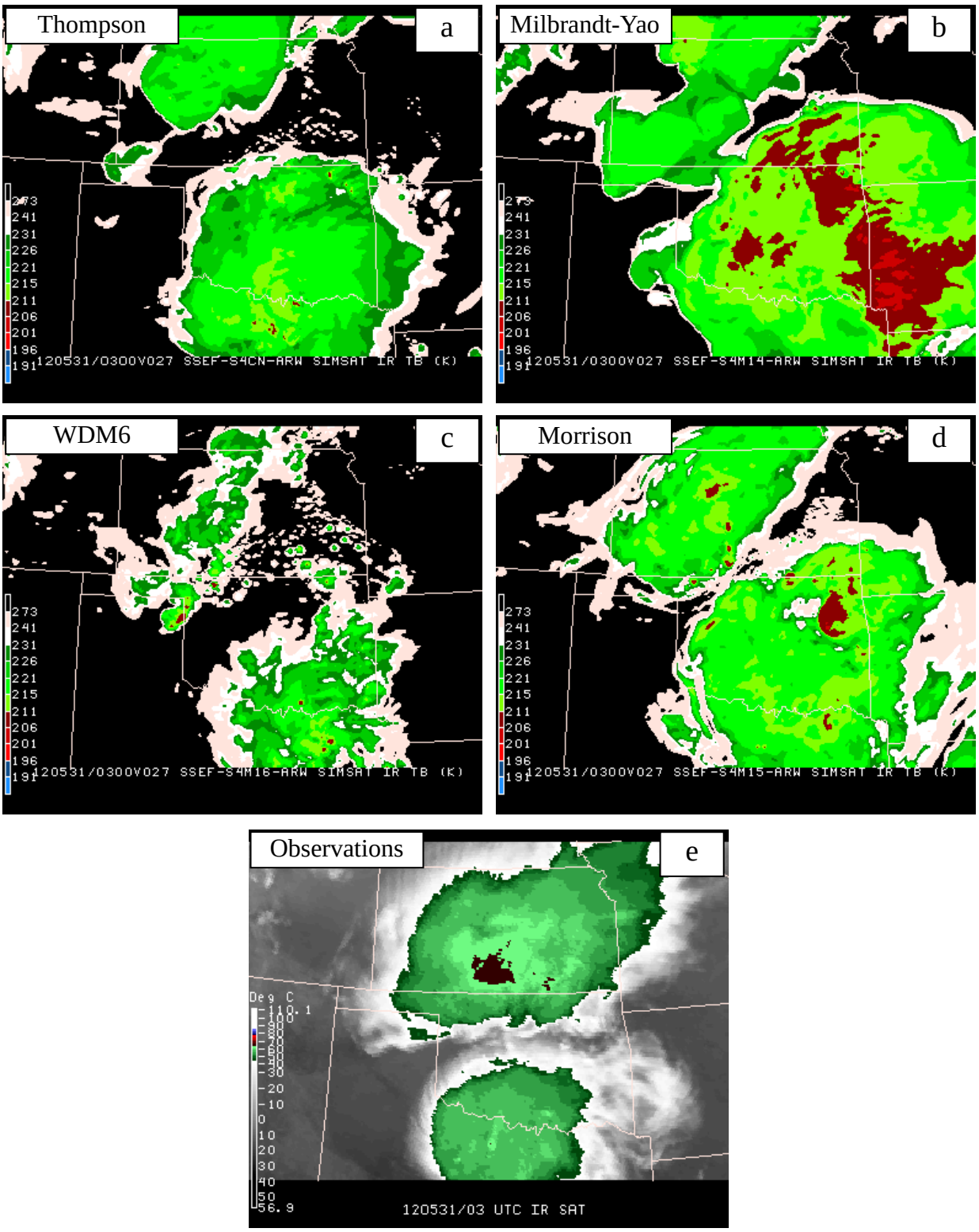

Fig. 11. *As in Fig. 8, but for the simulated and observed IR brightness temperature.*

6. SUMMARY

SFE12 was a multi-faceted experiment that brought together operational forecasters, scientific researchers, academics, and private sector meteorologists. Daily activities revolved around experimental forecasting exercises and systematic evaluation of new numerical guidance products and observational systems. Some of the experimental approaches were in the last stages of testing before operational implementation while others were in the early stages of development. An important result of the experiment was that it facilitated the migration of new strategies and guidance products from research to operations (R2O) and it helped to identify many areas where further research is needed (O2R). To give a few examples, on the forecasting side, the skillful performance of the SSEO was documented, providing compelling justification for its transition to forecasting operations at the SPC; on the research side, the relatively inexpensive *InterMet* sounding system was found to be suitable for future field experiments planned by NSSL and elsewhere, and an examination of sensitivities to MPs in CAMs highlighted many important sensitivities and areas where more research is needed. Thus, the HWT SFE continues to make a unique contribution to the meteorological community by promoting broad collaboration and important advances in operationally relevant research and scientifically informed forecasting operations.

Acknowledgements

Many individuals contributed to the success of SFE12, including Gregg Grosshans, Jay Liang, Joe Byerly, Brenda Gomez, and Peggy Stogsdill (SPC); Brett Morrow, Jeff Horn, Steve Fletcher, Brad Sagowitz, Greg Trotter, and Linda McGuckin (NSSL).

Authors Clark, Correia, Dembek, Lakshmanan, Marsh, Melick, Miller, and Sobash were partially funded by the NOAA/Office of Oceanic and Atmospheric Research under NOAA–University of Oklahoma Cooperative Agreement NA17RJ1227, U.S. Department of Commerce. CAPS ensemble forecasts were supported by the NOAA Collaborative Science, Technology, and Applied Research (CSTAR) Program with supplementary support from NSF grant AGS-0802888. M. Xue was also supported by NSF grants OCI-0905040, AGS-0941491, AGS-1046171, and AGS-1046081. CAPS forecasts were supported National Science Foundation XSEDE grant allocation and computations were performed at the National Institute for Computational Science. Many scientists at CAPS contributed to the design and production of the ensemble forecasts, including Yunheng Wang, Keith Brewster, Jidong Gao, and Xuguang Wang

Greg Thompson (NCAR) provided supplemental code for the WRF model and valuable insight that helped us compute simulated reflectivity from the different MP schemes in WRF properly. Hugh Morrison (NCAR), Jimy Dudhia (NCAR), Song-You Hong (Yonsei University), and Kyo-Sun Lim (Yonsei University) also contributed to this process.

References

Benjamin, S. G., and Coauthors, 2004: An hourly assimilation–forecast cycle: The RUC. *Mon. Wea. Rev.*, **132**, 495–518. doi: http://dx.doi.org/10.1175/1520-0493(2004)132<0495:AHACTR>2.0.CO;2

Bikos, D., D. T. Lindsey, J. Otkin, J. Sieglaff, L. Grasso, C. Siewert, J. Correia Jr., M. Coniglio, R. Rabin, J. S. Kain, S. Dembek, 2012: Synthetic satellite imagery for real-time high-resolution model evaluation. *Wea. Forecasting*, **27**, 784-795.

Chen, F., and J. Dudhia, 2001: Coupling an advanced land surface–hydrology model with the Penn State–NCAR MM5 modeling system. Part I: Model description and implementation. *Mon. Wea. Rev.*, **129**, 569–585.

Chen, S., and Coauthors, 2003: COAMPS version 3 model description: General theory and equations. *Naval Research Laboratory Tech. Rep.* NRL/PU7500-04-448, 141 pp.

Chou, M.-D., and M. J. Suarez, 1994: An efficient thermal infrared radiation parameterization for use in general circulation models. NASA Tech. Memo. 104606,85 pp. [Available from NASA Center for Aero Space Information, 800 Elkridge Landing Road, Linthicum Heights, MD 21090-2934.]

Clark, A. J., J. S. Kain, P. T. Marsh, J. Correia, Jr., M. Xue, and F. Kong, 2012a: Forecasting tornado path lengths using a 3-dimensional object identification algorithm applied to convection-allowing forecasts. *Wea. Forecasting,* **27**, 1090–1113.

Clark, A. J., J. S. Kain, T. L. Jensen, R. G. Bullock, M. Xue, and F. Kong, 2012b: Diagnosing sensitivities to microphysics parameterizations in convection-allowing models using object-based time-domain diagnostics. *Extended Abstracts, 26th Conference on Severe Local Storms*, Nashville, TN, Amer. Meteor. Soc., Paper 15.1

Coniglio, M. C., M. W. Douglas, D. D. Turner, and M. Fuentes, 2012: Evaluation of experimental

atmospheric profiling systems and WRF-ARW PBL schemes during the 2012 NOAA/HWT Experimental Forecast Program. *Extended Abstracts, 26th Conference on Severe Local Storms*, Nashville, TN, Amer. Meteor. Soc., Paper P9.4

Coniglio, M.C., J. Correia Jr., P. T. Marsh, and F. Kong, 2013: Verification of convection-allowing WRF model forecasts of the planetary boundary layer using sounding observations. *Wea. Forecasting*, **28**, 842-862.

Du, J. and Coauthors, 2009: NCEP Short-Range Ensemble Forecast (SREF) system upgrade in 2009. Extended Abstracts, 19th Conf. on Numerical Weather Prediction and 23rd Conf. on Weather Analysis and Forecasting, Omaha, NE, Amer. Meteor. Soc., 4A.4. [Available online at http://ams.confex.com/ams/23WAF19NWP/techprogram/paper_153264.htm.]

Ferrier, B. S., Y. Jin, Y. Lin, T. Black, E. Rogers, and G. DiMego, 2002: Implementation of a new grid-scale cloud and precipitation scheme in the NCEP Eta Model. *15th Conf. on Num. Weather Pred.*, San Antonio, TX.

Gao, J.-D., M. Xue, K. Brewster, and K. K. Droegemeier, 2004: A three-dimensional variational data analysis method with recursive filter for Doppler radars. *J. Atmos. Oceanic Technol.*, **21**, 457–469.

Gremillion, M. S. and R. E. Orville, 1999: Thunderstorm characteristics of cloud-to-ground lightning at the Kennedy Space Center, Florida: A study of lightning initiation signatures as indicated by the WSR-88D. *Wea. Forecasting*, **14**, 640-649

Hong, S.-Y., J. Dudhia, and S.-H. Chen, 2004: A revised approach to ice microphysical processes for the bulk parameterization of clouds and precipitation. *Mon. Wea. Rev.*, **132**, 103–120.

Hong, S.-Y., and J.-O. Lim, 2006: The WRF single-moment 6-class microphysics scheme (WSM6). *J. Korean Meteor. Soc.*, **42**, 129–151.

Janjic, Z.I., 1994: The step-mountain eta coordinate model: Further developments of the convection, viscous sublayer, and turbulence closure schemes. *Mon. Wea. Rev.*, **122**, 927-945.

Janjic´, Z. I., 2003: A nonhydrostatic model based on a new approach. *Meteor. Atmos. Phys.*, **82**, 271–285

Jirak, I. L., S. J. Weiss, and C. J. Melick, 2012a: The SPC Storm-Scale Ensemble of Opportunity: Overview and Results from the 2012 Hazardous Weather Testbed Spring Forecasting Experiment. *Extended Abstracts, 26th Conference on Severe Local Storms*, Nashville, TN, Amer. Meteor. Soc., Poster 137.

Jirak, I. L., C. J. Melick, A. R. Dean, and S. J. Weiss, and 2012b: Investigation of an Automated Temporal Disaggregation Technique for Convective Outlooks during the 2012 Hazardous Weather Testbed Spring Forecasting Experiment. *Extended Abstracts, 26th Conference on Severe Local Storms*, Nashville, TN, Amer. Meteor. Soc., Paper 10.2

Kain, J. S., S. J. Weiss, D. R. Bright, M. E. Baldwin, J. J. Levit, G. W. Carbin, C. S. Schwartz, M. L. Weisman, K. K. Droegemeier, D. B. Weber, K. W. Thomas, 2008: Some practical considerations regarding horizontal resolution in the first generation of operational convection-allowing NWP. *Wea. Forecasting*, **23**, 931-952.

Kain, J. S., S. R. Dembek, S. J. Weiss, J. L. Case, J. J. Levit, and R. A. Sobash, 2010: Extracting unique information from high resolution forecast models: Monitoring selected fields and phenomena every time step. *Wea. Forecasting*, **25**, 1536-1542.

Kain, J. S., M. C. Coniglio, J. Correia, A. J. Clark, P. T. Marsh, C. L. Ziegler, V. Lakshmanan, S. D. Miller, S. R. Dembek, S. J. Weiss, F. Kong, M. Xue, R. A. Sobash, A. R. Dean, I. L. Jirak, and C. J. Melick, 2013: A Feasibility Study for Probabilistic Convection Initiation Forecasts Based on Explicit Numerical Guidance. *Bull Amer. Meteor. Soc.*, in press.

Kong, F., and Coauthors, 2008: Real-time storm-scale ensemble forecast experiment—Analysis of 2008 spring experiment data. *Preprints, 24th Conf. on Severe Local Storms*, Savannah, GA, Amer. Meteor. Soc., 12.3. [Available online at http://ams.confex.com/ams/pdfpapers/141827.pdf.]

Kong, F., M. Xue, K. W. Thomas, Y. Wang, K. Brewster, A. J. Clark, J. S. Kain, S. J. Weiss, I. L. Jirak, M. C. Coniglio, J. Correia Jr., and P. Marsh, 2012: CAPS storm-scale ensemble forecasting system for the NOAA HWT 2012 Spring Experiment: Impact of IC/LBC perturbations. *Extended Abstracts, 26th Conference on Severe Local Storms*, Nashville, TN, Amer. Meteor. Soc., Paper P9.6

Lim, K.-S. S., and S.-Y. Hong, 2010: Development of an effective double-moment cloud microphysics scheme with prognostic cloud condensation nuclei (CCN) for weather and climate models. *Mon. Wea. Rev.*,**138**, 1587–1612.

Löhnert, U., D. D. Turner, S. Crewell, 2009: Ground-based temperature and humidity profiling using spectral infrared and microwave observations. Part I: Simulated retrieval performance in clear-sky conditions. *J. Appl. Meteor. Climatol.*, **48**, 1017–1032. doi: http://dx.doi.org/10.1175/2008JAMC2060.1

Marsh, P. T., J. S. Kain, A. J. Clark, V. Lakshmanan, G. Thompson, S. R. Dembek, S.

D. Miller Jr., M. C. Coniglio, J. Correia Jr., F. Kong, K. W. Thomas, and M. Xue, 2012: Objective Diagnosis of Thunderstorms and Convection Initiation Using Convection-Allowing Numerical Weather Prediction Models. *26th Conference on Severe Local Storms*, Nashville, TN, Amer. Meteor. Soc., Poster 134.

McCormick, J. R., E. L. Kuchera, and S. Rentschler, 2012: Ensemble forecast products for the 14 April 2012 severe weather event in Nebraska. *26th Conference on Severe Local Storms*, Nashville, TN, Amer. Meteor. Soc., Poster 113.

Mecikalski, J. R., K. M. Bedka, 2006: Forecasting convective initiation by monitoring the evolution of moving cumulus in daytime GOES imagery. *Mon. Wea. Rev.*, **134**, 49–78.

Melick,C.J, I.L. Jirak, A.R. Dean, J. Correia Jr, and S.J. Weiss, 2012: Real time objective verification of convective forecasts: 2012 HWT Spring Forecast Experiment. *Preprints, 37th Natl. Wea. Assoc. Annual Meeting*, Madison, WI, Natl. Wea. Assoc*.,* P1.52.

Milbrandt, J. A., M. K. Yau, 2005: A multimoment bulk microphysics parameterization. Part II: A proposed three-moment closure and scheme description. *J. Atmos. Sci.*, **62**, 3065–3081. doi: http://dx.doi.org/10.1175/JAS3535.1

Miller, S. D., Jr., J. S. Kain, P. T. Marsh, A. J. Clark, M. C. Coniglio, V. Lakshmanan, J. Correia Jr., D. A. Imy, S. R. Dembek, I. L. Jirak, S. J. Weiss, A. R. Dean, C. J. Melick, R. Sobash, M. Xue, F. Kong, and K. W. Thomas, 2012: Assessment of timing and coverage of convection during the 2012 NOAA Hazardous Weather Testbed Spring Forecasting Experiment. *Extended Abstracts, 26th Conference on Severe Local Storms*, Nashville, TN, Amer. Meteor. Soc., Paper 10.3

Miller, S. D., Jr., 2013: Exploration of new methods for predicting convective initiation. M. S. Thesis, University of Oklahoma School of Meteorology.

Mlawer, E. J., S. J. Taubman, P. D. Brown, M. J. Iacono, and S. A. Clough, 1997: Radiative transfer for inhomogeneous atmospheres: RRTM, a validated correlated-k model for the longwave. *J. Geophys. Res.*, **102**, 16 663–16 682.

Morrison, H., J. A. Curry, and V. I. Khvorostyanov, 2005: A new double-moment microphysics parameterization for application in cloud and climate models, Part I: Description. *J. Atmos. Sci.*, **62**, 1665–1677.

Nakanishi, M., and H. Niino, 2009: Development of an improved turbulence closure model for the atmospheric boundary layer. *J. Meteor. Soc. Japan*, **87**, 895–912.

Nash, J., R. Smout, T. Oakley, P. Pathack, and S. Kurnosenko, 2005: WMO intercomparison of high quality radiosonde systems, Vacoas, Mauritius, 2–25 February 2005. WMO Commission on Instruments and Methods of Observation, Final Rep., 118 pp. [Available online at http://www.wmo.ch/pages/prog/www/IMOP/reports/2003-2007/RSO-IC-2005_Final_Report.pdf.]

Noh, Y., W. G. Cheon, S.-Y. Hong, and S. Raasch, 2003: Improvement of the K-profile model for the planetary boundary layer based on large eddy simulation data. *Bound.-Layer Meteor.*, **107**, 401–427.

Otkin, J. A., D. C. Hartung, D. D. Turner, R. A. Petersen, W. F. Feltz, and E. Janzon, 2011: Assimilation of surface-based boundary layer profiler observations during a cool-season weather event using an observing system simulation experiment. Part I: Analysis impact. *Mon. Wea. Rev.*, **139**, 2309–2326. doi: http://dx.doi.org/10.1175/2011MWR3622.1

Pleim, J. E., 2007: A combined local and nonlocal closure model for the atmospheric boundary layer. Part I: Model description and testing. *J. Appl. Meteor. Climatol.*, **46**, 1383–1395.

Roberts, R. D., S. Rutledge, 2003: Nowcasting storm initiation and growth using GOES-8 and WSR-88D data. *Wea. Forecasting*, **18**, 562–584.

Rogers, E., and Coauthors, 2009: The NCEP North American Mesoscale modeling system: Recent changes and future plans. *Preprints, 23rd Conference on Weather Analysis and Forecasting/19th Conference on Numerical Weather Prediction*, Omaha, NE, Amer. Meteor. Soc., 2A.4.

Shutts, G. J., 2005: A kinetic energy backscatter algorithm for use in ensemble prediction systems. *Quart. J. Roy. Meteor. Soc.*, **131**, 3079–3102.

Skamarock, W. C., J. B. Klemp, J. Dudhia, D. O. Gill, D. M. Barker, M. G. Duda, X.-Y., Huang, W. Wang, and J. G. Powers, 2008: A description of the Advanced Research WRF Version 2, NCAR Tech Note, NCAR/TN-475+STR, 113 pp. [Available at: http://www.mmm.ucar.edu/wrf/users/docs/arw_v3.pdf.]

Smirnova, T. G., J. M. Brown, and S. G. Benjamin, 1997: Evolution of soil moisture and temperature in the MAPS/RUC assimilation cycle. *Preprints, 13th Conf. on Hydrology*, Long Beach, CA, Amer. Meteor. Soc., 172 – 175.

Smirnova, T. G., S. G. Benjamin, J. M. Brown, B. Schwartz, and D. Kim, 2000: Validation of long-term precipitation and evolved soil moisture and temperature fields in MAPS. *Preprints, 15th Conf. on Hydrology*, Long Beach, CA, Amer. Meteor. Soc., 43–46.

Sukoriansky, S., B. Galperian, and V. Perov, 2005: Application of a new spectral theory of stable stratified turbulence to the atmospheric

boundary layer over sea ice. *Bound.-Layer Meteor.*, **117**, 231–257.

Thompson, G., P. R. Field, W. R. Hall, and R. Rasmussen, 2008: Explicit forecasts of winter precipitation using an improved bulk microphysics scheme. Part II: Implementation of a new snow parameterization. *Mon. Wea. Rev.*, **136**, 5095–5115.

Xue, M., and Coauthors, 2001: The Advanced Regional Prediction System (ARPS)—A multi-scale nonhydrostatic atmospheric simulation and prediction tool. Part II: Model physics and applications. *Meteor. Atmos. Phys*., **76**, 143–165.

Xue, M., D.-H. Wang, J.-D. Gao, K. Brewster, and K. K. Droegemeier, 2003: The Advanced Regional Prediction System (ARPS), storm-scale numerical weather prediction and data assimilation. *Meteor. Atmos. Phys.*, **82**, 139–170.

Xue, M., and Coauthors, 2008: CAPS realtime storm-scale ensemble and high-resolution forecasts as part of the NOAA Hazardous Weather Testbed 2008 Spring Experiment. *Preprints, 24th Conf. on Severe Local Storms*, Savannah, GA, Amer. Meteor. Soc., 12.2. [Available online at http://ams.confex.com/ams/pdfpapers/142036.pdf.]